Supplementary Materials

The Se-S bond formation in the covalent inhibition mechanism of SARS-CoV-2 main protease by ebselen-like inhibitors. A computational study

Angela Parise[1,2], Isabella Romeo[1], Nino Russo[1] and Tiziana Marino [1*]

[1] Dipartimento di Chimica e Tecnologie Chimiche, Università della Calabria, Via Pietro Bucci, 87036 Arcavacata di Rende, CS, Italy
[2] Université Paris-Saclay, CNRS, Institut de Chimie Physique UMR8000, Orsay, France
* Correspondence: tiziana.marino65@unical.it

Table of Contents

Molecular Dynamics procedure

Molecular Dynamics analysis

Scheme S1. Proposed mechanism for the covalent inhibition of M^{pro}

Figure S1. Superposition of crystallographic structures

Figure S2. MD most populated structures

Figure S3. RMSD analysis

Figure S4. RMSF analysis

Figure S5. Pocket volume cavity

Figure S6. SASA

Figure S7. Catalytic dyad distance

Figure S8. Salt bridge

Figure S9. RDF water

Figure S10. Docking protocol setting

Figure S11. Best docked poses

Figure S12. Specific distances M^{pro} –EBS

Figure S13. Specific distances M^{pro} –EBS-OH

Figure S14. Optimized structures of HIE stationary points

Figure S15. Free energy profiles of M^{pro} HIE

Table S1. pKa values

Table S2. Donor-Acceptor H-bond M^{pro} HID

Table S3. Donor-Acceptor H-bond M^{pro} HIE

Table S4. RMSD-based clustering

Table S5. Docking scores

Table S6. NBO charges of EBS and EBS-OH

Table S7. NBO charges by atoms (M^{pro} HID – EBS)

Table S8. NBO charges by atoms (M^{pro} HIE – EBS)

Table S9. NBO charges by atoms (M^{pro} HID – EBS-OH)

Table S10. Energy values corrected including free energy (kcal/mol) in gas phase for the three used basis sets for the inhibition phase

References

Molecular Dynamics procedure

The crystal structure of main protease bound to potent broad-spectrum non-covalent inhibitor X77 with PDB code 6W63[1] were used as starting point. The structure is characterized by one chain of 306 amino acids. The apo-enzyme was obtained by removing the inhibitor from the crystallographic structure. The structure thus obtained was superimposed on other crystallographic structures (PDB codes: 6LU7[2] and 6Y2F[3]) with an RMSD value lower than 1 Å. (Figure S1).

The absent hydrogen atoms were added using H++ server[4] to calculate the protonation states of titratable residues at pH 7.4 (Table S1). The protonation states of the catalytic residue neutral His41, with the hydrogen on the side chain Nε (HIE) and Nδ (HID), have been considered. 300 ns MDs were performed for apo-M^{pro}, in the two protonation states (HIE and HID).

Each system has been solvated in an orthorhombic box with a buffer of 10 Å, using TIP3P water model. Na^+ ions have been added to ensure zero total charge. The solvated structure was minimized in stages using AMBER 16.[5] In particular, water molecules and counterions were minimized over 2500 steps of steepest descent and 2500 steps of conjugate gradient minimization with a 50 kcal mol^{-1} $Å^{-2}$ constraint on the solute. Subsequentially, hydrogen atoms were minimized over 5000 steps of steepest descent and 5000 steps of conjugate gradient with a 50 kcal mol^{-1} $Å^{-2}$ constraint on all heavy atoms. Next, 5000 steps of steepest descent and 5000 steps of conjugate gradient minimization was performed, with 50 kcal mol^{-1} $Å^{-2}$ constraint on protein backbone. Finally, the whole system has been released with 3000 and 6000 steps of unconstrained steepest descent and conjugate gradient respectively. Each stage of minimization was run until the root-mean-square of the Cartesian gradient was low than 10^{-4} kcal mol^{-1} $Å^{-1}$. Then a progressive heating phase was carried out from 0 to 310 K for 0.5 ns using the Langevin thermostat (g = 2.0) in NVT ensemble. The production phase consist of 300 ns of MDs using FF14SB force field[6] under the following conditions: integration step of 2 fs coupling SHAKE algorithm; NPT ensemble at 1 bar pressure using the Berendsen barostat[7] with a time constant τp = 2.0 ps. The Particle mesh Ewald summation method[8] has been employed for the electrostatic potential long-range interactions with a 12 Å cut-off distance.

In order to select different representative conformations of the system, root-mean square deviation (RMSD) based clustering of the whole trajectory has been performed using the an agglomerative bottom-up approach (hieragglo algorithm) available in Amber16 tools. After removing overall rotations and translations by RMS-fitting the Cα atoms' positions of the trajectory, the average linkage clustering algorithm has been applied, identifying 10 representative conformations of the protein (Figure S2 and Table S2).

Afterwards, the representative structures with the highest percentage of population (Table S2) were considered for the further molecular docking studies, performed by using AutoDock (version 4.2).[9]

The ligands (EBS and EBS-OH) and the SARS-CoV-2 M^{pro} models, apo-HID and apo-HIE, were processed using the AutoDock Tools [9] to obtain the PDBQT (Protein Data Bank, Partial Charge (Q), & Atom Type (T)) coordinate files containing the information needed by AutoGrid and AutoDock, namely polar hydrogen atoms, partial charges, correct atom types, and information on the articulation of flexible molecules. In order to verify if the adopted docking procedure is adequate, we have performed the docking of X77 inhibitor present in the used crystallographic structure. The results, reported in Figure S10 (as docking protocol setting) return a good superposition with a RMSD of 1.91 Å. In particular, Gasteiger-Marsili charges[10] were loaded in ADT (Auto Dock Tools). The center of the grid box locates on the sulfur atom of Cys145, and a dimension box of 70x70x70 Å has been chosen to abundant cover the active site. For ligand conformational searching the Lamarckian genetic algorithm (LGA)[11] has been used. The docking conditions were as follows: 10 independent runs, population size of 150, random starting position and conformation, local search rate of 0.6 and 2500000 energy evaluations. Final docked poses have been clustered using RMSD tolerance of 0.5 Å (Table S5).

The best docking pose was chosen according to the most negative docking score (Figure S11).

In order to obtain ebselen-like compound (EBS and EBS-OH) parameters gas phase geometry optimization has been carried out using B3LYP/6-31G*. Atomic charges are derived by fitting the electrostatic potential according to the Merz−Singh−Kollman scheme,[12] using the RESP fitting procedure. Antechamber and parmchk modules of Amber16 has been used for generating preparatory files to perform MM relaxation of the complexes HID-EBS, HIE-EBS and HID-EBS-OH.

Molecular Dynamics analysis

Root-mean-square deviation (RMSD) of the protein M^{pro} HID and M^{pro} HIE backbone, RMSD of the active site, root mean square fluctuation (RMSF), solvent accessible surface area (SASA), radial distribution function (RDF), hydrogen (H)-bond analysis and RMSD-based clustering MD simulation were performed using cpptraj module of AmberTools 16.[5] Electrostatic calculations were performed with the Adaptive Poisson-Boltzmann Solver (APBS).[13] Volume cavity of the binding pocket was performed with CAVER 2.0 Analyst[14] , a very rough estimation of the volume. The volume of the pocket ,in cubic Å, is computed by random sampling the bounding box of filling balls with a radius of 5 Å.

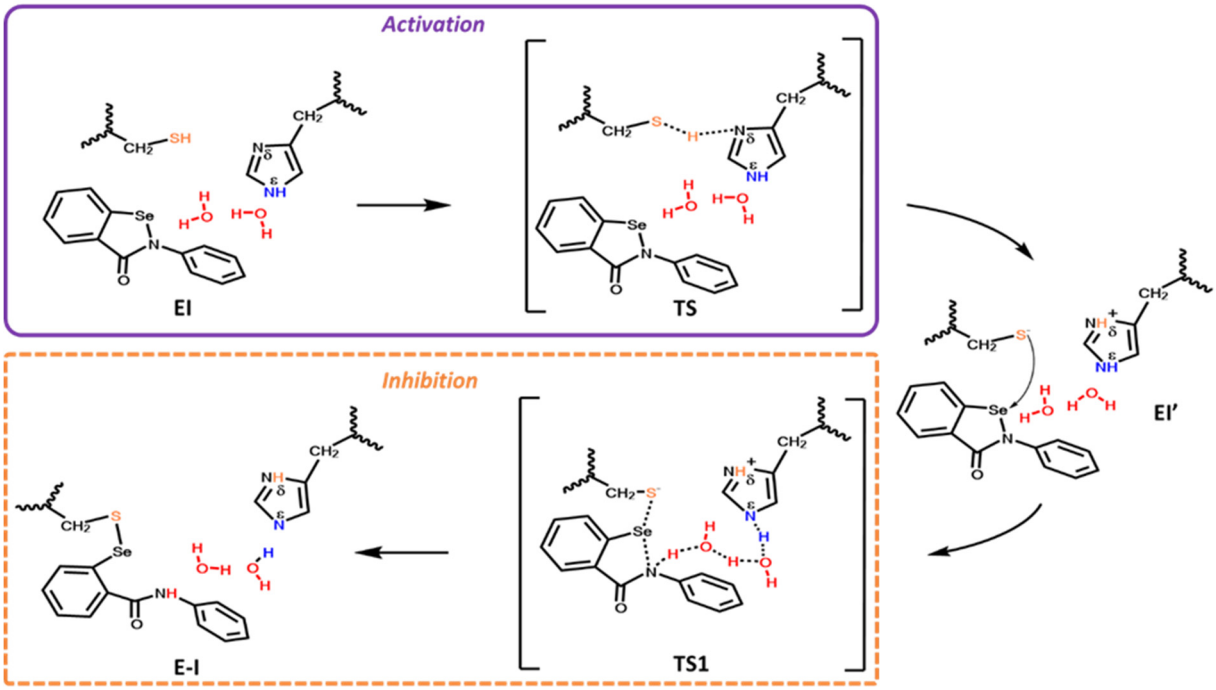

Scheme S1. *Proposed mechanism for the covalent inhibition of M^pro SARS-CoV-2 for HIE by EBS in two phases: activation (in violet) and inhibition through covalent bond formation (in dashed orange).*

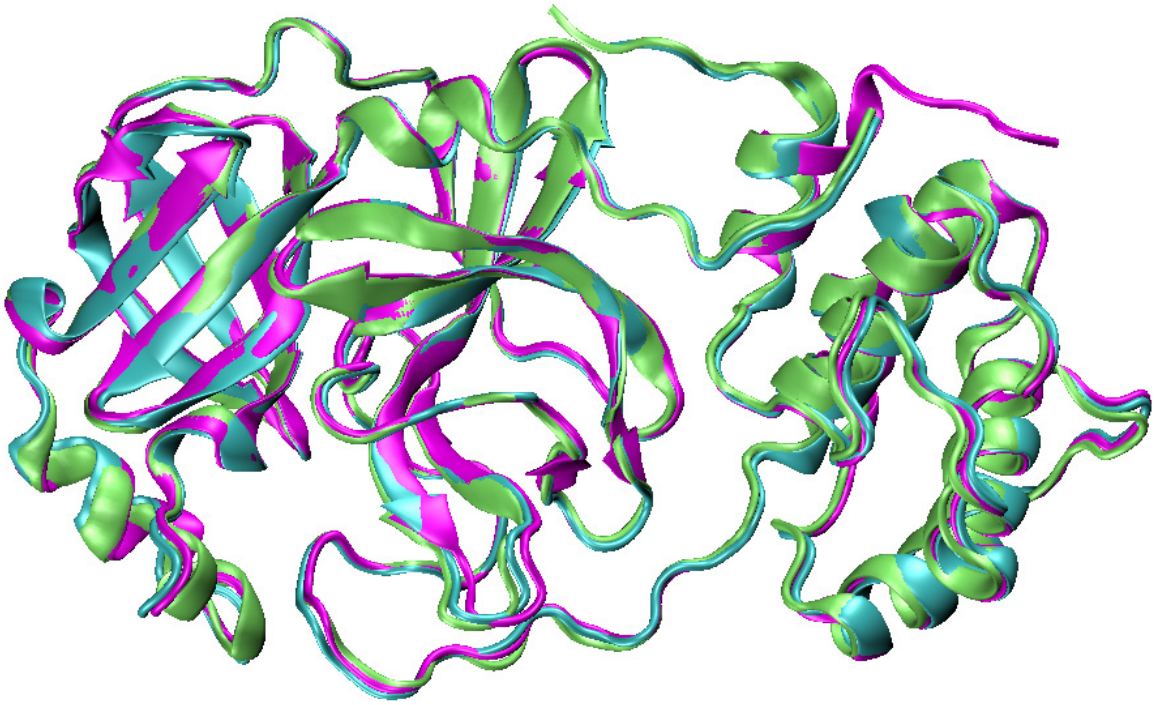

Figure S1. Superposition of M^pro crystallographic structures: 6W63 in cyano, 6LU7 in magenta, and 6Y2F in lime.

a)

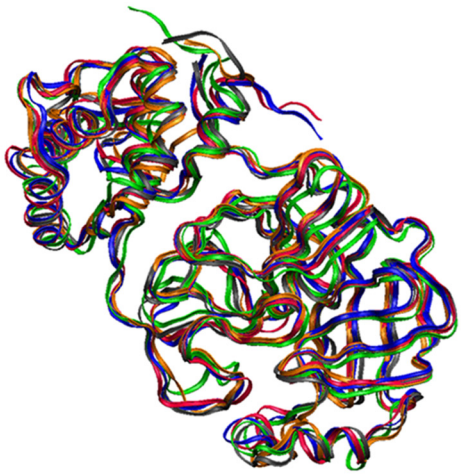

b)

Structure	Color	RMSD
Cluster 0	Gray	2.70
Cluser 1	Orange	2.78
Cluster 2	Green	3.59
Cluster 3	Red	1.19
Xray	Blue	-

a')

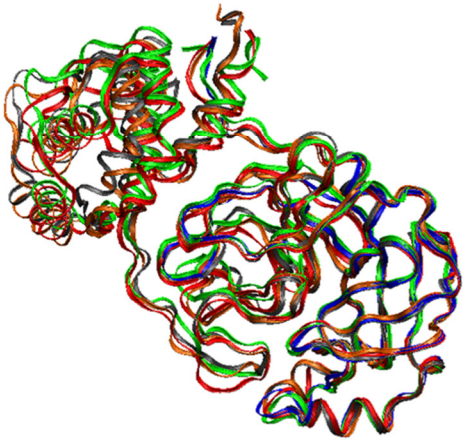

b')

Structure	Color	RMSD
Cluster 0	Gray	2.26
Cluser 1	Orange	2.11
Cluster 2	Green	1.77
Cluster 3	Red	1.74
Xray	Blue	-

Figure S2. Superposition of 4 most populated structures obtained by RMSD-based clustering MD simulation of **(**a) M^{pro} HIE and (a') M^{pro} HID. RMSD values of HIE clusters (b) with respect to X-Ray 6W63, RMSD values of HID clusters (b') with respect to X-Ray 6W63.

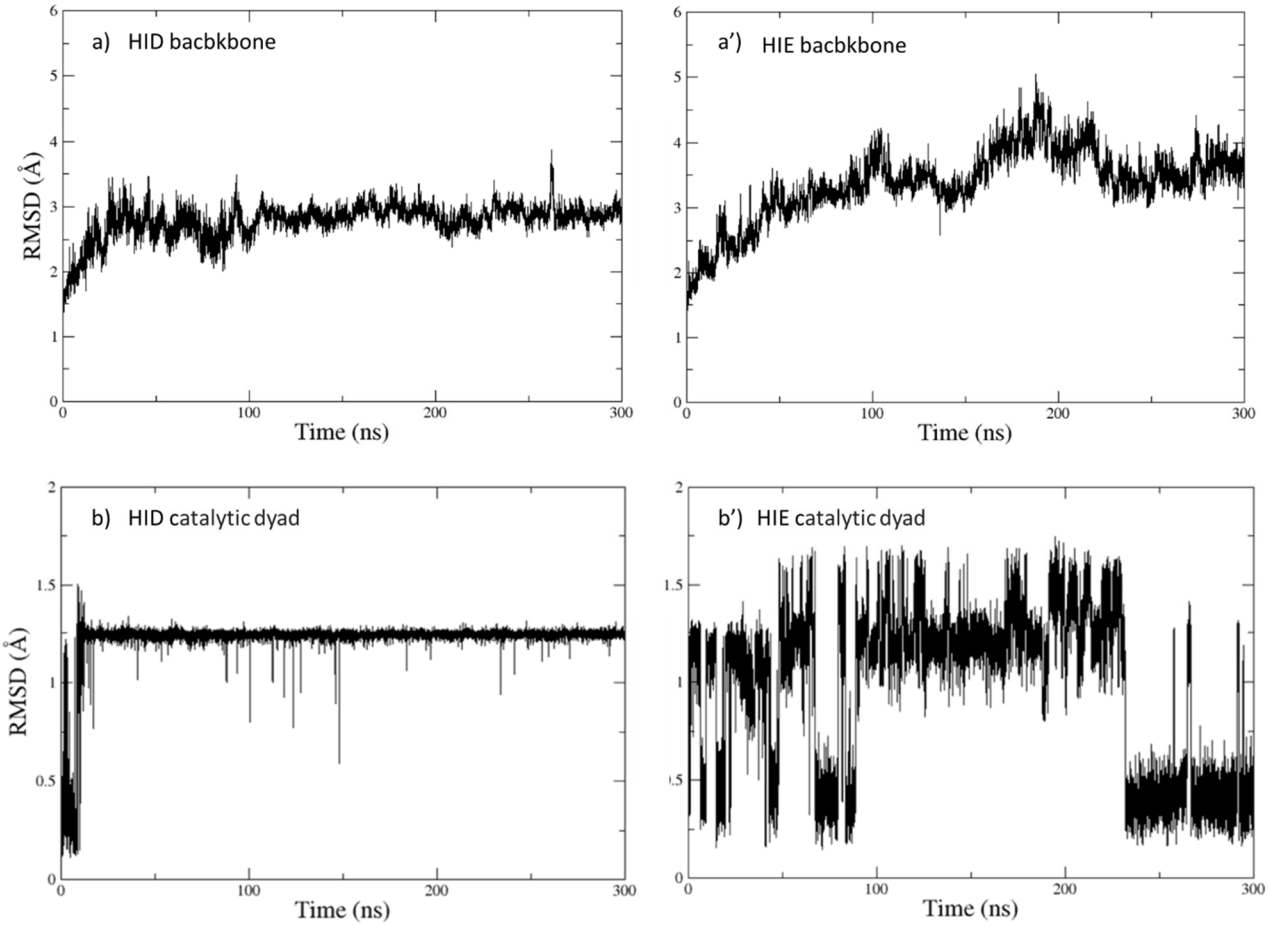

Figure S3. Up: backbone RMSD trend of a) M^{pro} (HID) and a′) M^{pro} (HIE) along MD simulation time, expressed in Å. Down: RMSD trend of residues His41 and Cys145 b) M^{pro} (HID) and b′) M^{pro} (HIE).

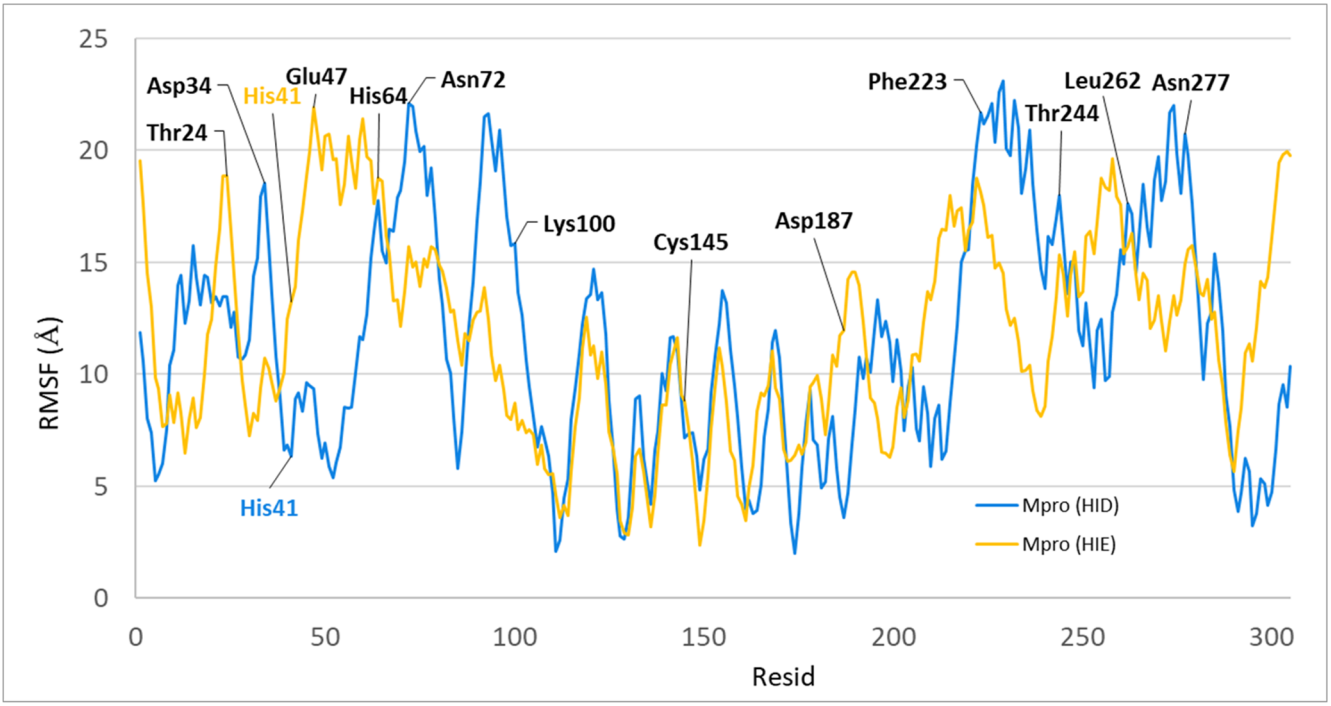

Figure S4. RMSF comparison between M^{pro} (HID) in blue and M^{pro} (HIE) in yellow; some residues with high DRMSF value between the two protonation states of His41 simulations are explicitly reported in the graph.

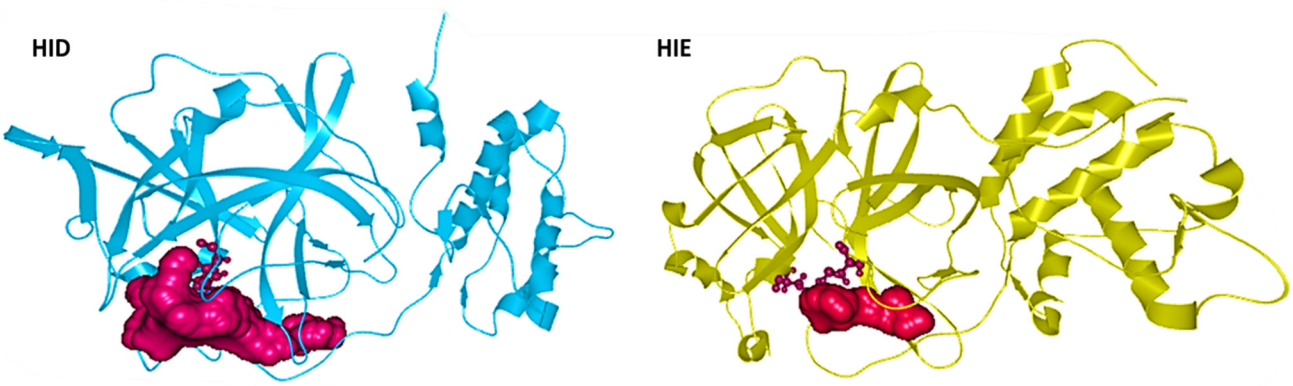

Figure S5. Pocket volume cavity of binding site: value of 598.1 $Å^3$ for M^{pro} HID (in blue) and value of 227.7 Å3 M^{pro} HIE (in gold). The calculation was performed with CAVER Analyst 2.0. 5 Å sphere size used to define the pocket of each system for volume calculations.

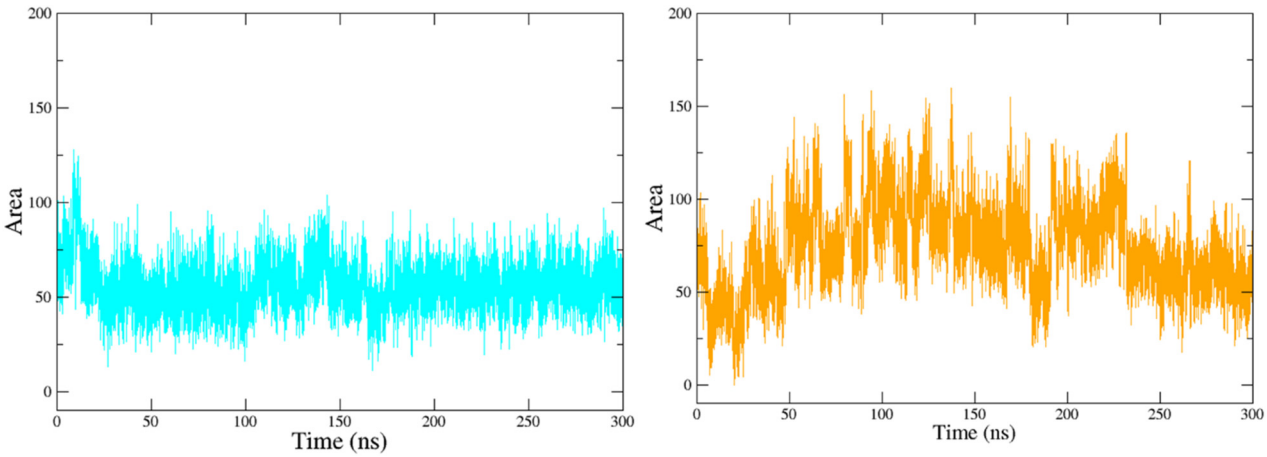

Figure S6. Solvent accessibility surface area (SASA) along the trajectory, expressed in Å^2 and calculated based on the residues Cys145 and His41 in different protonation states: HID in orange and HID in blue. SASA was calculated with CPPTRAJ using LCPO algorithm.[15]

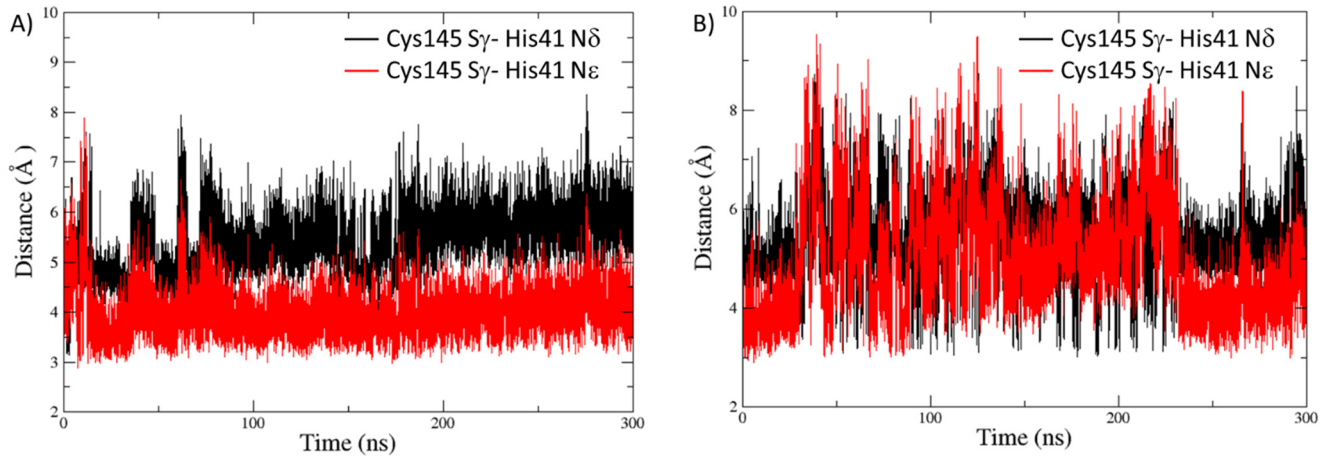

Figure S7. Distance between N and S (red) and N and S (black) in the catalytic residues His41 and Cys145. Graph A) refers to HID and graph B) refers to HIE trajectories.

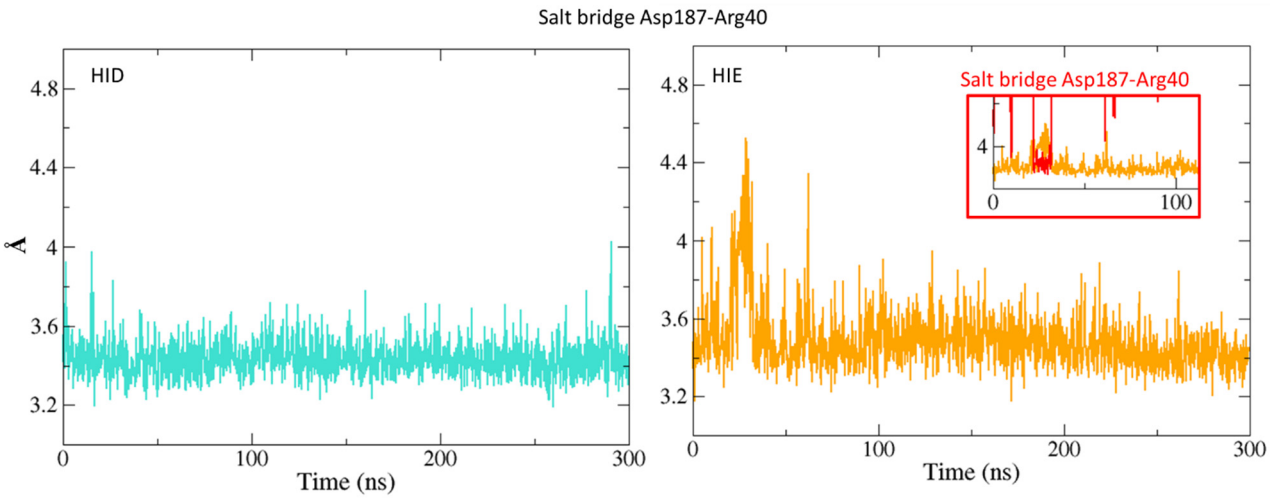

Figure S8. Salt bridges between residues Asp186 and Arg40 along the MD simulation trajectory, for HID and HIE, cyano and orange respectively. For the HIE trajectory, an additional data of salt bridge Asp187-Arg40 is zoom and shown in the red square. Analysis was performed by VMD plugin Version 1.1 with the cutoff distance of 3.2 Å.

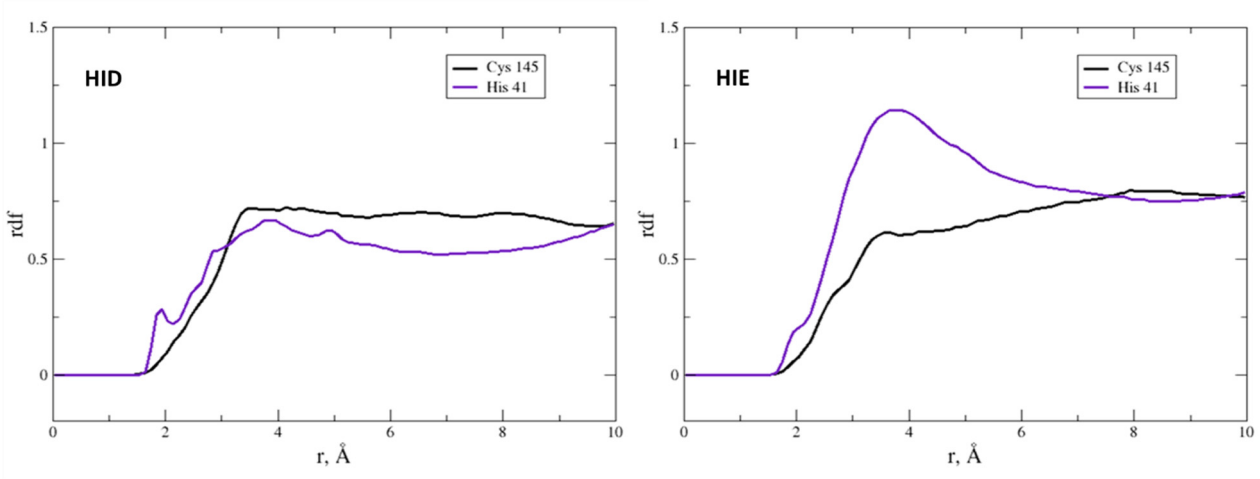

Figure S9. Water radial distribution function (RDF) analysis obtained as function of the distance (r) expressed in Å between water oxygen and side chains of Cys145 (black line) and His41 (purple line), for HID on left and for HIE on right.

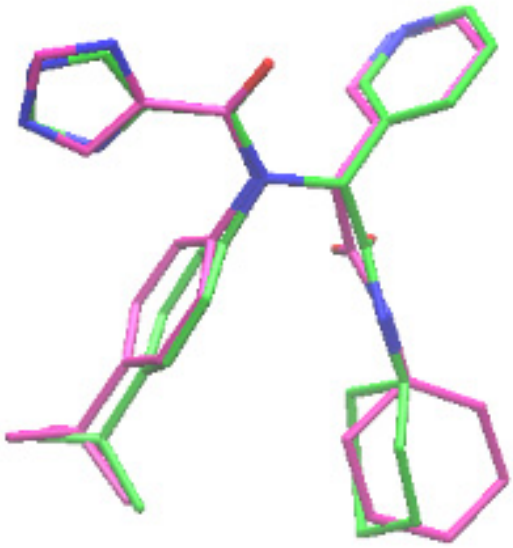

Figure S10. Superposition of **X77** structure obtained by the best docking pose (in pink) and X-Ray structure (colored by atom) with a RMSD of 1.91 Å.

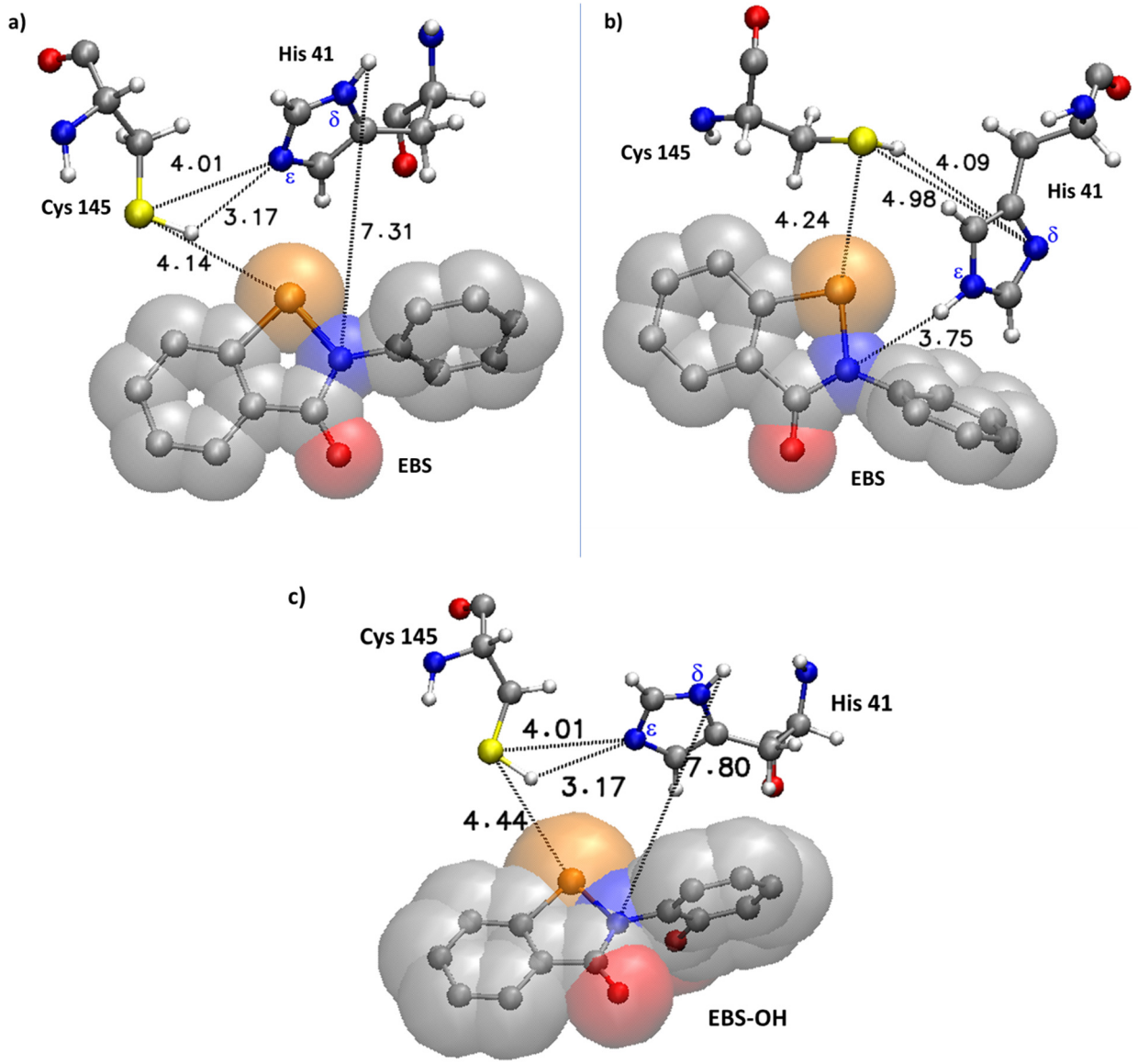

Figure S11. Structure and main distances (in Å) between atoms of M^{pro} active site and inhibitor best docked pose, a) refers to EBS docked in the M^{pro} HID most populeted cluster, b) refers to EBS docked in the M^{pro} HIE most populeted cluster and c) is the best docked pose of EBS-OH in the catalitic pocket of M^{pro} HID; van der Waals radii of EBS and EBS-OH atoms are shown in transparent.

HID-EBS	EI	TS	EI'	TS1	E-I
d (O-ND2) Å	2.94	3.13	2.99	3.10	2.78
d' (O-HD22) Å	1.95	2.25	2.12	2.22	1.75

HIE-EBS	EI	TS	EI'	TS1	E-I
d (O-ND2) Å	4.49	4.49	3.83	3.60	3.13
d' (O-HD22) Å	3.93	3.12	3.33	3.11	2.46

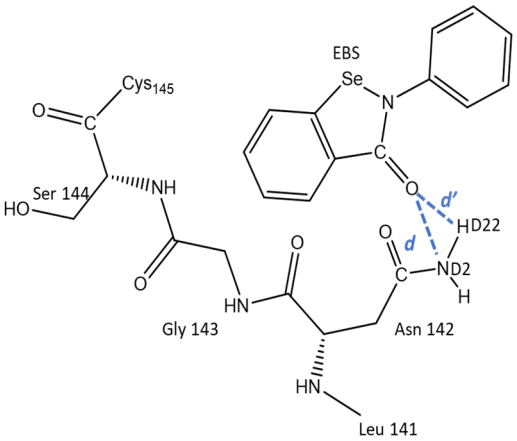

Figure S12. Tables containing distances between EBS oxygen atom and Asn 142 atoms ND2 (d) and HDD2 (d') as depicted in the included scheme on the right. Table on top refers to HID; table down refers to HIE.

HID-EBS-OH	EI	TS	EI'	TS1	E-I
d (O-ND2) Å	5.95	3.04	3.02	2.83	2.73
d' (O-HD22) Å	5.12	2.66	2.42	1.83	1.74
d (H-OG) Å	1.77	1.67	1.68	1.88	1.81

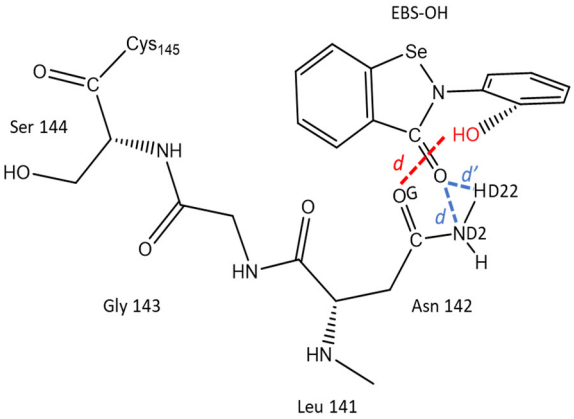

Figure S13. Tables containing distances between some selected atoms of EBS-OH and Asn 142 side chain. Distance between carbonyl oxygen O of EBS-OH and Asn 142 ND2 (d)/HDD2 (d') are in blue, ditance between H of EBS-OH hydroxyl group and OG of Asn 142 is in red, as depicted in the included scheme on the right.

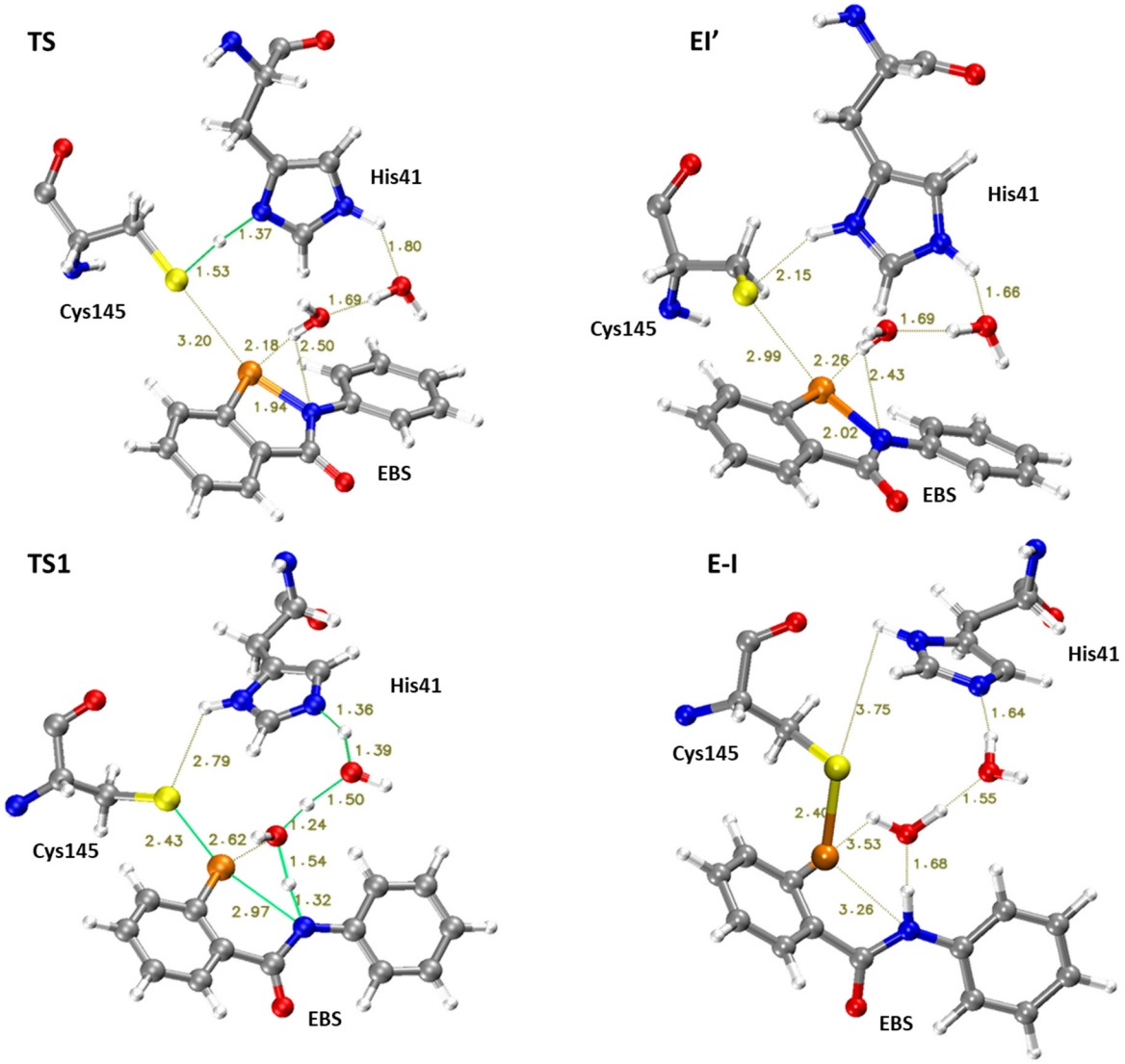

Figure S14. Optimized structures of the stationary points involved in the M^{pro} HIE inhibition process promoted by EBS. For clarity, only residues of the model implicated in the chemical event are shown. Main distances are in Å. Imaginary frequencies are reported in cm^{-1} for all transition states.

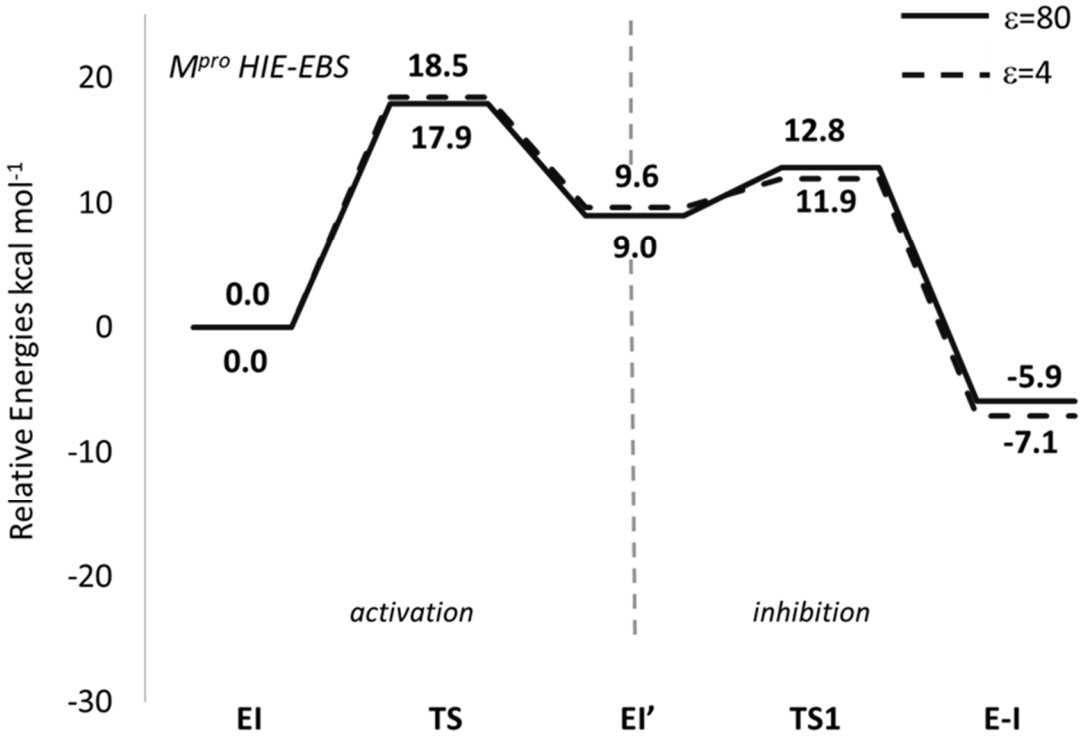

Figure S15. B3LYP-D3/6-31+G (2d,2p) free energy profiles of M^{pro} HIE SARS-CoV-2 covalent inhibition mechanism by EBS in two phases: activation and inhibition through covalent bond formation, expressed in kcal mol-1. Solid line indicates calculations in water (Ɛ=80) and dotted line in protein environment (Ɛ=4).

Table S1. Calculated pKa for ionizable residues of M^{pro}. Residues fully protonated (positively charged) and deprotonated (negatively charged) are colored in blue and red respectively. Residues belonging to the catalytic dyad are in bold.

	pKa	**Residue**	***pKa***
Arg4	11.81	Asp153	4.40
Lys5	8.45	Tyr154	9.67
Lys12	9.30	Asp155	4.37
Glu14	3.81	Cys156	9.62
Cys16	12.15	Cys160	10.25
Cys22	11.90	Tyr161	11.64
Asp33	3.87	His163	4.17
Asp34	4.50	His164	3.75
Tyr37	11.32	Glu166	4.67
Cys38	12.12	His172	4.08
Arg40	11.20	Asp176	2.86
His41	**4.42**	Glu178	3.92
Cys44	9.99	Tyr182	13.32
Glu47	4.10	Asp187	5.09
Asp48	3.37	Arg188	11.61
Tyr54	13.17	Asp197	4.16
Glu55	4.55	Tyr209	13.34
Asp56	4.46	Asp216	4.29
Arg60	12.16	Arg217	11.81
Lys61	10.19	Arg222	11.97
His64	6.37	Asp229	4.15
Arg76	11.77	Lys236	10.40
His80	7.39	Tyr237	10.96
Cys85	10.18	Tyr239	11.16
Lys88	10.65	Glu240	4.60
Lys90	10.18	Asp245	3.56
Asp92	3.81	His246	3.97
Lys97	10.43	Asp248	4.05
Lys100	10.04	Asp263	3.92
Tyr101	10.51	Cys265	11.78
Lys102	9.91	Lys269	9.18
Arg105	11.70	Glu270	4.58
Cys117	10.91	Arg279	12.06
Tyr118	11.68	Glu288	4.07
Tyr126	13.65	Asp289	3.38
Cys128	10.29	Glu290	4.52
Arg131	10.66	Asp295	4.14
Lys137	9.56	Arg298	10.30
Cys145	**8.94**	Cys300	10.05

Table S2. Donor-Acceptor hydrogen bond details of 300 ns M^{pro} HID simulation. Only H-bonds involving the side chains atoms of amino acid residues have been reported It also shows the occupancy of each hydrogen bond.

A residue	A atom	D residue	D atom	Freq
GLU240	O	THR201	OG1	0 .9789
ASN133	OD1	THR135	OG1	0 .9790
CYS160	O	TYR182	OH	0 .9791
ASP176	O	THR175	OG1	0 .9793
ASP187	OD1	ARG40	NH2	0 .9794
ASP263	O	SER267	OG	0 .9797
ASP187	**OD2**	**ARG40**	**NE**	**0 .9798**
ASN28	OD1	GLY120	N	0 .9804
ILE259	O	SER254	OG	0 .9807
ILE259	O	TYR209	OH	0 .9808
PHE181	O	ARG105	NH2	0 .9811
LEU253	O	THR257	OG1	0 .9812
LEU141	O	SER144	OG	0 .9815
GLN127	OE1	SER113	OG	0 .9819
ASP289	O	ASN203	ND2	0 .9821
TRP31	O	ASN95	ND2	0 .9824
GLY195	O	ASN133	ND2	0 .9836
ASN231	OD1	LEU242	N	0 .9838
CYS145	O	ASN28	ND2	0 .9841
ASP289	OD2	ARG131	NH2	0 .9844
ASP295	OD2	THR111	OG1	0 .9852
ASN180	O	ARG105	NH1	0 .9863
ASN65	OD1	SER62	N	0 .9868
SER113	OG	PHE8	N	0 .9870
ASN95	OD1	LYS97	N	0 .9878
THR280	O	TRP218	NE1	0 .9883
ASP176	OD2	ARG105	NH1	0 .9885
ALA210	O	ASN214	ND2	0 .9886
LEU286	O	SER284	OG	0 .9887

Table S3. Donor-Acceptor hydrogen bond details of 300 ns M^{pro} HIE simulation. Only H-bonds involving the side chains atoms of amino acid residues have been reported. It also shows the occupancy of each hydrogen bond.

A residue	A atom	D residue	D atom	Freq
CYS160	O	TYR182	OH	0.9519
GLU240	O	THR201	OG1	0.9502
ASP263	O	SER267	OG	0.8845
ASN133	OD1	THR135	OG1	0.8843
ASP176	O	THR175	OG1	0.8626
ASP187	OD1	ARG40	NH2	0.8189
ILE259	O	TYR209	OH	0.7847
ASN28	OD1	GLY120	N	0.7741
ILE259	O	SER254	OG	0.7659
LEU253	O	THR257	OG1	0.7652
LEU141	O	SER144	OG	0.7566
ASN231	OD1	LEU242	N	0.7233
TRP31	O	ASN95	ND2	0.7071
THR175	O	MET162	N	0.7016
ASP187	OD2	ARG40	NE	0.6625
ASP289	O	ASN203	ND2	0.6545
PHE181	O	ARG105	NH2	0.6023
CYS145	O	ASN28	ND2	0.5805
SER144	O	SER147	OG	0.5753
ASP48	OD2	THR45	OG1	0.5590
LEU286	O	SER284	OG	0.5453
ASN95	OD1	LYS97	N	0.5163
ASP176	OD1	ASN180	N	0.5045

Table S4. Tables of 10 structures obtained by RMSD-based clustering of MD simulations. M^{pro} HID (top) and M^{pro} HIE (down). From first column: cluster name, number of frames included in the cluster, population respect to total processed frames in percentage, average distance between frames inside the cluster expressed in Å, standard deviation related to Avg d and the centroid frame.

Name	Frames	Pop %	Avg d (Å)	σ	Centroid
Cluster 0	6594	44.0	2.09	0.40	9055
Cluster 1	3467	23.1	2.06	0.41	10699
Cluster 2	1978	13.2	2.01	0.38	1017
Cluster 3	999	6.7	1.86	0.36	2320
Cluster 4	699	4.7	2.00	0.39	227
Cluster 5	675	4.5	1.90	0.39	469
Cluster 6	269	1.8	1.72	0.43	4677
Cluster 7	176	1.2	1.64	0.38	64
Cluster 8	108	0.7	1.37	0.19	13153
Cluster 9	35	0.2	0.00	0.00	16

Name	Frames	Pop %	Avg d (Å)	σ	Centroid
Cluster 0	5012	25.1	1.71	0.34	15341
Cluster 1	4213	21.1	1.86	0.39	7693
Cluster 2	3456	17.3	1.74	0.38	18467
Cluster 3	2302	11.5	1.60	0.33	939
Cluster 4	1553	7.8	1.66	0.37	9760
Cluster 5	1551	7.8	1.60	0.29	2581
Cluster 6	1276	6.4	1.50	0.25	4517
Cluster 7	323	1.6	1.38	0.26	3995
Cluster 8	290	1.5	1.38	0.30	17856
Cluster 9	25	0.1	0.00	0.00	2349

Table S5. Docking scores values related to the free energy of protein-ligand binding affinity expressed in kcal mol^{-1} and it's relative RMSD in Å. a) M^{pro} HID most representative cluster and EBS, b) M^{pro} HIE most representative cluster and EBS and c) M^{pro} HID with EBS-OH. Results are reported for all 10 docking poses ranked by energy. Best docking poses values are shown in red.

	a) M^{pro} HID and EBS		**b) M^{pro} HIE and EBS**		**c) M^{pro} HID and EBS-OH**	
Pose	E (kcal mol^{-1})	RMSD (Å)	E (kcal mol^{-1})	RMSD (Å)	E (kcal mol^{-1})	RMSD (Å)
1	-5.85	0.00	-6.39	0.00	-5.67	0.00
2	-5.85	0.02	-6.39	0.01	-5.48	1.59
3	-5.85	0.01	-6.39	0.02	-5.47	1.58
4	-5.85	0.06	-6.39	0.02	-5.27	1.75
5	-5.85	0.05	-6.38	0.11	-5.27	1.74
6	-5.85	0.05	-6.38	0.14	-5.26	1.73
7	-5.84	0.08	-6.38	0.12	-5.23	0.45
8	-5.84	0.07	-6.38	0.06	-5.21	1.71
9	-5.84	0.11	-6.38	0.09	-5.18	1.39
10	-5.55	0.00	-6.38	0.04	-5.04	1.37

Table S6. NBO charge values of heavy atoms in |e| for EBS and EBS-OH. Atoms numbering follows the sketch on the right.

	EBS	EBS-OH
Se 1	0.634	0.622
N 2	-0.602	-0.661
C 3	0.673	0.665
O 3	-0.618	-0.597
C 4	-0.177	-0.177
C 5	-0.252	-0.252
C 6	-0.213	-0.212
C 7	-0.257	-0.258
C 1'	0.152	0.053
C 2'	-0.254	-0.202
C 3'	-0.229	-0.270
C 4'	-0.250	-0.218
C 5'	-0.231	-0.285
C 6'	-0.273	0.322
O 6' (OH)	-	-0.702

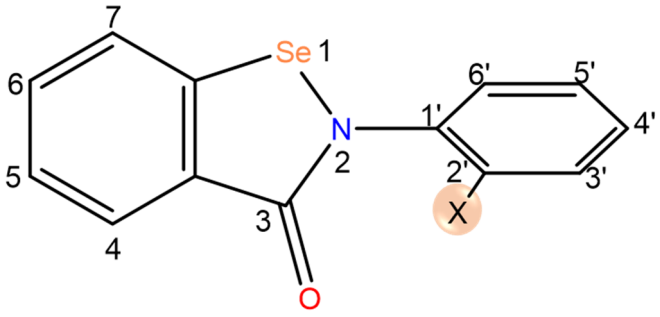

Table S7. NBO charge values of heavy atoms in |e| for every stationary point along the potential energy surface of inhibition promoted by EBS on M^{pro} HID. Heavy atoms of the inhibitor, of the two catalytic waters, of the catalytic dyad and of the residues immediately close to the dyad are reported.

Residue	Atom	EI	TS	EI'	TS1	E-I
His 41	N	-0.100	-0.027	-0.002	-0.224	-0.066
His 41	CA	0.591	0.123	-0.015	0.181	0.337
His 41	CB	-0.912	-0.857	-0.727	0.124	-0.885
His 41	CG	0.515	0.599	0.375	0.145	-0.079
His 41	ND1	-0.219	-0.003	-0.007	0.152	-0.193
His 41	CE1	0.469	0.135	0.908	0.315	0.266
His 41	NE2	-0.223	0.274	-0.026	0.066	0.086
His 41	CD2	0.069	0.189	0.374	0.139	0.639
His 41	C	0.163	0.410	0.464	0.597	0.236
His 41	O	-0.375	-0.424	-0.427	-0.598	-0.364
Asn 142	N	0.044	-0.088	-0.097	-0.181	0.140
Asn 142	CA	0.068	0.683	0.691	0.252	-0.109
Asn 142	CB	-0.231	-0.312	-0.326	-0.025	-0.273
Asn 142	CG	0.813	0.550	0.541	0.949	0.853
Asn 142	OD1	-0.472	-0.454	-0.449	-0.788	-0.464
Asn 142	ND2	0.029	0.126	0.123	-0.180	0.134
Asn 142	C	0.073	-0.306	-0.290	0.791	-0.081
Asn 142	O	-0.475	-0.510	-0.516	-0.752	-0.435
Gly 143	N	0.259	0.170	0.174	-0.313	0.129
Gly 143	CA	-0.171	0.075	0.074	0.296	-0.267
Gly 143	C	0.345	0.181	0.173	0.836	0.680
Gly 143	O	-0.338	-0.402	-0.405	-0.704	-0.492
Ser 144	N	0.217	0.215	0.226	-0.405	0.311
Ser 144	CA	0.113	0.364	0.384	0.240	0.343
Ser 144	CB	-0.039	0.123	0.115	0.387	-0.174
Ser 144	OG	-0.107	-0.098	-0.099	-0.298	-0.093
Ser 144	C	0.479	0.141	0.115	1.043	0.178
Ser 144	O	-0.533	-0.572	-0.585	-0.925	-0.511
Cys 145	N	0.298	0.373	0.344	-0.509	0.407
Cys 145	CA	0.683	-0.135	-0.290	0.196	0.530
Cys 145	CB	-0.782	-0.528	-0.500	0.061	-0.495
Cys 145	SG	0.143	-0.074	0.542	-0.461	-0.077
Cys 145	C	-0.092	0.129	0.439	1.020	-0.447
Cys 145	O	-0.414	-0.387	-0.527	-0.960	-0.389
Gly 146	N	0.086	0.068	0.074	-0.473	0.099
Gly 146	CA	0.163	0.189	0.178	0.260	0.149
Gly 146	C	0.471	0.477	0.475	0.694	0.498
Gly 146	O	-0.415	-0.402	-0.407	-0.653	-0.397
EBS	C5	-0.154	-0.109	-0.119	-0.038	0.217
EBS	C6	0.257	-0.194	-0.238	0.058	-0.017
EBS	C4	-0.224	-0.518	-0.520	0.083	-0.742
EBS	C7	0.353	0.737	0.806	-0.128	0.981

EBS	C(-CO)	-0.797	0.068	0.028	-0.196	0.287
EBS	C(-Se)	0.586	-0.248	-0.287	0.153	-0.761
EBS	C3	0.004	-0.354	-0.346	0.929	1.042
EBS	N2	-0.265	-0.002	0.011	-0.378	0.162
EBS	O	-0.460	-0.530	-0.546	-0.860	-0.506
EBS	Se1	0.343	0.614	0.714	0.666	-0.258
EBS	C1’	-1.152	-0.077	-0.129	0.332	-0.748
EBS	C6’	1.461	0.307	0.329	-0.048	-0.230
EBS	C5’	-0.946	-0.416	-0.434	-0.004	0.279
EBS	C4’	0.420	0.176	0.160	-0.053	0.211
EBS	C3’	-0.525	0.052	0.052	0.011	-0.208
EBS	C2’	0.750	0.344	0.326	-0.033	0.550
W1	O	0.071	0.085	0.082	-0.846	-0.053
W2	O	0.085	0.053	0.103	0.058	0.070

Table S8. NBO charge values of heavy atoms in |e| for every stationary point along the potential energy surface of inhibition promoted by EBS on M^{pro} HIE. Heavy atoms of the inhibitor, of the two catalytic waters, of the catalytic dyad and of the residues immediately close to the dyad are reported.

Residue	Atom	EI	TS	EI'	TS1	E-I
His 41	N	-0.609	-0.576	-0.583	-0.585	-0.584
His 41	CA	0.003	-0.029	-0.005	-0.005	-0.014
His 41	CB	-0.310	-0.327	-0.332	-0.333	-0.327
His 41	CG	0.128	0.182	0.080	0.302	0.266
His 41	ND1	-0.570	-0.580	-0.430	-0.697	-0.720
His 41	CE1	0.228	0.342	0.232	0.369	0.365
His 41	NE2	-0.704	-0.666	-0.667	-0.612	-0.578
His 41	CD2	0.087	0.095	0.111	0.016	0.002
His 41	C	0.377	0.388	0.352	0.347	0.381
His 41	O	-0.421	-0.425	-0.418	-0.403	-0.418
Asn 142	N	-0.538	-0.539	-0.536	-0.527	-0.537
Asn 142	CA	-0.040	-0.040	-0.050	-0.060	-0.038
Asn 142	CB	-0.317	-0.317	-0.312	-0.323	-0.328
Asn 142	CG	0.547	0.551	0.539	0.559	0.575
Asn 142	OD1	-0.508	-0.511	-0.498	-0.508	-0.536
Asn 142	ND2	-0.719	-0.718	-0.716	-0.715	-0.681
Asn 142	C	0.521	0.497	0.513	0.524	0.507
Asn 142	O	-0.503	-0.486	-0.491	-0.494	-0.493
Gly 143	N	-0.655	-0.656	-0.666	-0.648	-0.645
Gly 143	CA	-0.126	-0.176	-0.182	-0.166	-0.171
Gly 143	C	0.546	0.553	0.509	0.535	0.540
Gly 143	O	-0.497	-0.511	-0.456	-0.518	-0.521
Ser 144	N	-0.604	-0.608	-0.640	-0.616	-0.605
Ser 144	CA	-0.092	-0.052	-0.080	-0.066	-0.058
Ser 144	CB	-0.031	-0.042	-0.024	-0.034	-0.041
Ser 144	OG	-0.619	-0.624	-0.635	-0.616	-0.620
Ser 144	C	0.602	0.579	0.603	0.548	0.570
Ser 144	O	-0.567	-0.550	-0.495	-0.495	-0.539
Cys 145	N	-0.645	-0.622	-0.616	-0.641	-0.634
Cys 145	CA	-0.034	-0.030	-0.019	-0.043	-0.016
Cys 145	CB	-0.494	-0.473	-0.501	-0.486	-0.517
Cys 145	SG	0.009	-0.169	-0.430	-0.115	-0.110
Cys 145	C	0.546	0.555	0.551	0.551	0.557
Cys 145	O	-0.472	-0.487	-0.466	-0.484	-0.473
Gly 146	N	-0.654	-0.682	-0.633	-0.641	-0.683
Gly 146	CA	-0.178	-0.136	-0.182	-0.159	-0.140
Gly 146	C	0.360	0.346	0.368	0.352	0.351
Gly 146	O	-0.409	-0.411	-0.409	-0.394	-0.402
EBS	C5	-0.145	-0.142	-0.136	-0.132	-0.152
EBS	C6	-0.104	-0.111	-0.115	-0.112	-0.097
EBS	C4	-0.109	-0.117	-0.114	-0.120	-0.090
EBS	C7	-0.169	-0.146	-0.137	-0.157	-0.149

EBS	C(-CO)	0.115	0.127	0.093	0.039	0.047
EBS	C(-Se)	-0.381	-0.384	-0.395	-0.337	-0.248
EBS	C3	0.540	0.540	0.498	0.494	0.490
EBS	N2	-0.944	-0.924	-0.952	-0.789	-0.826
EBS	O	-0.467	-0.470	-0.430	-0.501	-0.424
EBS	Se1	0.705	0.633	0.619	0.389	0.321
EBS	C1’	0.334	0.341	0.286	0.304	0.458
EBS	C6’	-0.203	-0.193	-0.098	-0.167	-0.166
EBS	C5’	-0.158	-0.146	-0.137	-0.145	-0.141
EBS	C4’	-0.120	-0.116	-0.101	-0.114	-0.117
EBS	C3’	-0.169	-0.167	-0.147	-0.155	-0.115
EBS	C2’	-0.125	-0.120	-0.092	-0.099	-0.261
W1	O	-0.796	-0.811	-0.779	-0.818	-0.825
W2	O	-0.752	-0.759	-0.768	-0.769	-0.725

Table S9. NBO charge values of heavy atoms in |e| for every stationary point along the potential energy surface of inhibition promoted by EBS-OH on M^{pro} HID. Heavy atoms of the inhibitor, of the two catalytic waters, of the catalytic dyad and of the residues immediately close to the dyad are reported.

Residue	Atom	EI	TS	EI'	TS1	E-I
His 41	N	-0.046	0.053	0.053	-0.006	0.009
His 41	CA	0.360	-0.235	-0.007	-0.034	-0.009
His 41	CB	-0.796	-0.308	-0.942	-0.586	-0.141
His 41	CG	0.150	0.823	0.513	0.360	0.333
His 41	ND1	0.214	0.035	0.133	0.211	-0.044
His 41	CE1	0.129	0.146	0.374	0.046	-0.183
His 41	NE2	-0.212	-0.363	0.141	0.215	-0.217
His 41	CD2	0.209	-0.255	0.771	0.615	0.416
His 41	C	0.414	0.557	0.226	0.433	0.224
His 41	O	-0.343	-0.401	-0.368	-0.403	-0.369
Asn 142	N	0.114	0.090	0.109	-0.013	0.131
Asn 142	CA	-0.185	0.076	-0.237	0.191	-0.237
Asn 142	CB	-0.624	-0.137	-0.504	-0.812	-0.558
Asn 142	CG	1.218	0.628	1.019	1.304	1.119
Asn 142	OD1	-0.533	-0.514	-0.474	-0.456	-0.511
Asn 142	ND2	0.060	0.088	0.044	0.120	0.062
Asn 142	C	0.180	0.029	0.079	-0.036	0.433
Asn 142	O	-0.431	-0.441	-0.448	-0.516	-0.422
Gly 143	N	0.181	0.321	0.340	0.199	0.207
Gly 143	CA	-0.461	-0.386	-0.139	-0.193	-0.181
Gly 143	C	0.985	0.581	0.594	0.530	0.393
Gly 143	O	-0.324	-0.499	-0.477	-0.400	-0.468
Ser 144	N	0.380	0.363	0.282	0.290	0.285
Ser 144	CA	-0.229	0.276	0.085	-0.183	0.356
Ser 144	CB	-0.190	-0.098	-0.189	0.062	-0.120
Ser 144	OG	-0.058	-0.042	-0.069	-0.099	-0.065
Ser 144	C	0.335	0.278	0.221	0.586	0.318
Ser 144	O	-0.470	-0.517	-0.521	-0.573	-0.517
Cys 145	N	0.403	0.553	0.270	0.236	0.447
Cys 145	CA	0.689	0.397	1.013	0.063	0.857
Cys 145	CB	-0.509	-0.542	-0.932	-0.665	-1.122
Cys 145	SG	0.321	0.421	-0.552	0.305	0.847
Cys 145	C	-0.496	-0.593	-0.174	-0.037	-0.759
Cys 145	O	-0.411	-0.451	-0.432	-0.490	-0.463
Gly 146	N	0.123	0.134	0.106	0.080	0.166
Gly 146	CA	0.141	0.089	0.104	0.201	0.072
Gly 146	C	0.500	0.550	0.531	0.440	0.572
Gly 146	O	-0.414	-0.413	-0.431	-0.395	-0.419
EBS	C5	-0.022	-0.201	-0.077	-0.228	-0.231
EBS	C6	0.827	0.092	0.025	-0.225	-0.062
EBS	C4	0.119	0.167	0.325	0.364	-0.618
EBS	C7	0.025	-0.052	0.236	0.621	1.537

EBS	C(-CO)	-0.374	0.167	-0.496	-0.029	0.041
EBS	C(-Se)	0.727	0.179	-0.702	-0.791	-0.141
EBS	C3	0.521	0.130	0.210	0.812	0.084
EBS	N2	-0.129	0.540	-0.415	-0.740	0.341
EBS	O	-0.389	-0.388	-0.071	-0.458	-0.307
EBS	Se1	0.036	-0.393	-0.472	-0.178	-0.628
EBS	C1’	0.005	-0.999	-0.399	0.112	-0.578
EBS	C6’	-0.116	0.692	0.252	0.050	0.323
EBS	C5’	-0.142	-0.302	0.028	-0.077	-0.348
EBS	C4’	0.148	0.188	-0.118	0.181	0.280
EBS	C3’	0.137	-0.110	0.793	0.295	-0.038
EBS	C2’	-0.033	0.363	-0.065	-0.412	0.012
EBS	O (2')	-0.094	-0.050	-0.497	0.039	0.000
W1	O	-0.058	0.048	0.371	0.039	0.037
W2	O	-0.099	-0.366	0.622	0.037	-0.147

Table S10. Energy values corrected including free energy (kcal/mol) in gas phase for the three used basis sets for the inhibition phase

EBS	6-31+G	6-311+G(2d,p)	AUG-cc-pVTZ
EI	0.0	0.0	0.0
TS1	11.5	10.6	11.1
EBS-OH			
EI	0.0	0.0	0.0
EI’	-1.0	-1.2	-2.5
TS1	11.1	8.2	8.7

References

1 https://www.wwpdb.org/pdb?id=pdb_00006w63, 2020, .

2 Z. Jin, X. Du, Y. Xu, Y. Deng, M. Liu, Y. Zhao, B. Zhang, X. Li, L. Zhang, C. Peng, Y. Duan, J. Yu, L. Wang, K. Yang, F. Liu, R. Jiang, X. Yang, T. You, X. Liu, X. Yang, F. Bai, H. Liu, X. Liu, L. W. Guddat, W. Xu, G. Xiao, C. Qin, Z. Shi, H. Jiang, Z. Rao and H. Yang, *Nature*, 2020, **582**, 289–293.

3 L. Zhang, D. Lin, X. Sun, U. Curth, C. Drosten, L. Sauerhering, S. Becker, K. Rox and R. Hilgenfeld, 2020, **368**, 409−412.

4 R. Anandakrishnan, B. Aguilar and A. V. Onufriev, *Nucleic Acids Res*, 2012, **40**, W537-541.

5 Case, D. A.; Ben-Shalom, I. Y.; Brozell, S. R.; Cerutti, D. S.; Cheatham, T. E., III; Cruzeiro, V. W. D.; Darden, T. A.; Duke, R. E.; Ghoreishi, D.; Gilson, M. K.; Gohlke, H.; Goetz, A. W.; Greene, D.; Harris, R.; Homeyer, N.; Izadi, S.; Kovalenko, A.; Kurtzman, T.; Lee, T. S.; LeGrand, S.; Li, P.; Lin, C.; Liu, J.; Luchko, T.; Luo, R.; Mermelstein, D. J.; Merz, K. M.; Miao, Y.; Monard, G.; Nguyen, C.; Nguyen, H.; Omelyan, I.; Onufriev, A.; Pan, F.; Qi, R.; Roe, D. R.; Roitberg, A.; Sagui, C.; Schott-Verdugo, S.; Shen, J.; Simmerling, C. L.; Smith, J.; Salomon-Ferrer, R.; Swails, J.; Walker, R. C.; Wang, J.; Wei, H.; Wolf, R. M.; Wu, X.; Xiao, L.; York, D. M.; Kollman, P. A. AMBER 2017; University of California, San Francisco, 2017., .

6 J. A. Maier, C. Martinez, K. Kasavajhala, L. Wickstrom, K. E. Hauser and C. Simmerling, ff14SB, https://pubs.acs.org/doi/full/10.1021/acs.jctc.5b00255, (accessed 13 January 2021).

7 H. J. C. Berendsen, J. P. M. Postma, W. F. van Gunsteren, A. DiNola and J. R. Haak, *The Journal of Chemical Physics*, 1998, **81**, 3684.

8 T. Darden, D. York and L. Pedersen, *The Journal of Chemical Physics*, 1998, 98, 10089.

9 G. M. Morris, R. Huey, W. Lindstrom, M. F. Sanner, R. K. Belew, D. S. Goodsell and A. J. Olson, *Journal of Computational Chemistry*, **30**, 7.

10 J. Gasteiger and M. Marsili, *Tetrahedron*, 1980, **36**, 3219–3228.

11 G. M. Morris, D. S. Goodsell, R. S. Halliday, R. Huey, W. E. Hart, R. K. Belew and A. J. Olson, *JOURNAL OF COMPUTATIONAL CHEMISTRY*, **19**, 24.

12 C. I. Bayly, P. Cieplak, W. Cornell and P. A. Kollman, *J. Phys. Chem.*, 1993, **97**, 10269–10280.

13 N. A. Baker, D. Sept, S. Joseph, M. J. Holst and J. A. McCammon, *Proc Natl Acad Sci U S A*, 2001, **98**, 10037–10041.

14 E. Chovancova, A. Pavelka, P. Benes, O. Strnad, J. Brezovsky, B. Kozlikova, A. Gora, V. Sustr, M. Klvana, P. Medek, L. Biedermannova, J. Sochor and J. Damborsky, *PLoS Comput Biol*, 2012, **8**, e1002708.

15 J. Weiser, P. S. Shenkin and W. C. Still, *Journal of Computational Chemistry*, 1999, **20**, 217–230.